Optimal Design for Parameter Estimation in EEG Problems in a 3D Multilayered Domain

March 30, 2014

H.T. Banks [†], D. Rubio[‡] , N. Saintier[♭] , M.I. Troparevsky[♯]
[†]CRSC, North Carolina State University,USA, htbanks@ncsu.edu
[‡]Centro de Matemática Aplicada, Universidad de San Martín, Buenos Aires, ARG, diarubio@gmail.com
[♭]Instituto de Ciencias, Universidad Nacional Gral. Sarmiento, Buenos Aires, ARG, nsaintie@dm.uba.ar
[♯]Dep. de Matemática, Facultad de Ingeniería, Universidad de Buenos Aires, ARG, mariainestro@gmail.com

Abstract

The fundamental problem of collecting data in the "best way" in order to assure statistically efficient estimation of parameters is known as *Optimal Experimental Design*. Many inverse problems consist in selecting best parameter values of a given mathematical model based on fits to measured data. These are usually formulated as optimization problems and the accuracy of their solutions depends not only on the chosen optimization scheme but also on the given data. We consider an electromagnetic interrogation problem, specifically one arising in an electroencephalography (EEG) problem, of finding optimal number and locations for sensors for source identification in a 3D unit sphere from data on its boundary. In this effort we compare the use of the classical D-optimal criterion for observation points as opposed to that for a uniform observation mesh. We consider location and best number of sensors and report results based on statistical uncertainty analysis of the resulting estimated parameters.

Keywords: Electromagnetic inverse problems, optimal design in 3D EEG analysis, parameter estimation, asymptotic error analysis.

Report Documentation Page

Form Approved
OMB No. 0704-0188

1. REPORT DATE	2. REPORT TYPE	3. DATES COVERED
30 MAR 2014		**00-00-2014 to 00-00-2014**

4. TITLE AND SUBTITLE	5a. CONTRACT NUMBER
Optimal Design for Parameter Estimation in EEG Problems in a 3D Multilayered Domain	5b. GRANT NUMBER
	5c. PROGRAM ELEMENT NUMBER
6. AUTHOR(S)	5d. PROJECT NUMBER
	5e. TASK NUMBER
	5f. WORK UNIT NUMBER
7. PERFORMING ORGANIZATION NAME(S) AND ADDRESS(ES) **North Carolina State University,Center for Research in Scientific Computation,Raleigh,NC,27695**	8. PERFORMING ORGANIZATION REPORT NUMBER
9. SPONSORING/MONITORING AGENCY NAME(S) AND ADDRESS(ES)	10. SPONSOR/MONITOR'S ACRONYM(S)
	11. SPONSOR/MONITOR'S REPORT NUMBER(S)

12. DISTRIBUTION/AVAILABILITY STATEMENT
Approved for public release; distribution unlimited

13. SUPPLEMENTARY NOTES
Mathematical Biosciences and Engineering, submitted

14. ABSTRACT

The fundamental problem of collecting data in the est way" in order to assure statistically e cient estimation of parameters is known as Optimal Experimental Design. Many inverse problems consist in selecting best parameter values of a given mathematical model based on ts to measured data. These are usually formulated as optimization problems and the accuracy of their solutions depends not only on the chosen optimization scheme but also on the given data. We consider an electromagnetic interrogation problem, speci cally one arising in an electroencephalography (EEG) problem, of nding optimal number and locations for sensors for source identi cation in a 3D unit sphere from data on its boundary. In this e ort we compare the use of the classical D-optimal criterion for observation points as opposed to that for a uniform observation mesh. We consider location and best number of sensors and report results based on statistical uncertainty analysis of the resulting estimated parameters.

15. SUBJECT TERMS

16. SECURITY CLASSIFICATION OF:			17. LIMITATION OF ABSTRACT	18. NUMBER OF PAGES	19a. NAME OF RESPONSIBLE PERSON
a. REPORT **unclassified**	b. ABSTRACT **unclassified**	c. THIS PAGE **unclassified**	**Same as Report (SAR)**	**25**	

1 Introduction

In a series of recent works [6, 7, 8, 11, 12] several authors have developed a design framework based on the Fisher Information Matrix (FIM) for a system of differential equations to determine when and where an experimenter should take samples and what variables to measure in collecting information on a physical or biological process that is modeled by a vector dynamical system. This framework has also been proposed for use in inverse problem methodologies in the context of dynamical system or mathematical model parameter estimation when one investigates the sufficiency of the number of observations of one or more states (variables). Experimental design using the Fisher Information Matrix (FIM), which is based on sensitivity functions (traditional and generalized), is described in [7] for the case of scalar data. In [8], the authors develop an experimental design theory using the FIM to identify optimal sampling times for experiments on physical processes (modeled by an ODE system) in which scalar or vector data will be taken. The methodology can be readily applied to problems involving ordinary, partial and delay differential equations dynamics but requires both a *mathematical model* and a *statistical model*. Early efforts published in this area were concerned with parameter estimation for one dimensional dynamic systems in one space or time dimension. More recently, these ideas were successfully applied in [11] for an experimentally validated six-compartment HIV model and a thirty-eight dimensional enzyme kinetics model of the Calvin Cycle in spinach.

In [13] and [14] proof-of-concept numerical results for a distributed parameter system in a 3D *one layer spherical domain* are presented for several different design criteria (D-optimal, SE-optimal, IGSF-optimal). In this present effort, a more general case in 3D is studied. Motivated again by classical problems in EEG analysis, we consider a stationary process modeled by a Poisson type equation with *multiple interfaces* given by

$$\nabla \cdot (\kappa(x)\nabla u(x,\theta)) \quad = \quad g(x,\theta) \quad x \in \Omega. \tag{1}$$

Here $\theta \in \mathbb{R}^p$ is the parameter to be estimated, Ω is the multilayered sphere in $\mathbb{R}^3$, $\kappa(x)$ is a piecewise positive constant conductivity function, $u(x,\theta) \in \mathbb{R}$, $x \in \partial\Omega$ is the output and $g : \mathbb{R}^{3+p} \to \mathbb{R}$ is the source. For this investigation we suppose that there exists a real value θ_0 such that the equation (1) accurately describes the process.

For the estimation process, we formulate a statistical model [35] of the form (absolute error)

$$Y(x) \quad = \quad u(x,\theta_0) + \mathcal{E}(x), \quad x \in \partial\Omega, \tag{2}$$

where θ_0 is the vector of true values of the unknown parameters and $\mathcal{E}$ is a vector random process that represents observation error for the measured variables. Realizations of the statistical model (2) can be written as

$$y(x) \quad = \quad u(x,\theta_0) + \epsilon(x), \quad x \in \partial\Omega. \tag{3}$$

In almost every real problem only a discrete set of output data is available. We denote $\{y_1, ..., y_n\}$ the measurements at $\Lambda = \{x_1, \ldots, x_n\} \subset \partial\Omega$. In this context, the parameter value θ_0 may be estimated by an Ordinary Least Square (OLS) procedure yielding an estimate $\hat{\theta}$. That is,

$$\hat{\theta} = \arg\min_{\theta \in \mathcal{A}} J_\Lambda(\theta)$$

where $\mathcal{A}$ is the set of admisible parameter values and $J_\Lambda(\theta)$ denotes the square errors between the measured and simulated outputs at the observation points, i.e.,

$$J_\Lambda(\theta) = \sum_{j=1}^{n} |u(x_j,\theta) - y_j|^2. \tag{4}$$

Different choices of the points $x_1, \ldots, x_n \in \Lambda$ may lead to different estimates, and thus it is important to look for the *optimal* set of observation points that will lead to an accurate parameter estimation. This is the purpose of the so-called *Optimal Design* methods, like D-Optimal, SE-Optimal, E-optimal design methods (see [6, 7]). For the sake of clarity, in the remainder of this article we omit the subindexes Λ on J.

The results presented here will clearly illustrate the advantages of performing some type of design such as D-Optimal design in connection to the estimation of the parameters in the problem described by (1).

2 The EEG Inverse Problem

The electrical activity of the brain consists of currents generated by biochemical sources at the cellular level. The electric and magnetic fields that they produce can be estimated by means of Maxwell equations (see [27, 33]). Based on the properties of the tissues involved, the velocity of propagation of the electromagnetic waves caused by potential changes within the brain is such that the effect may be detected simultaneously at any point in the brain or in the surrounding tissues. This fact justifies the use of a static approximation of Maxwell equations. This approximation uncouples the equations for the magnetic and electric fields leading to a 3D Poisson-type equation with interfaces that relates the electric potential u in the head with the impressed current C.

The equation that relates the electric potential u and the impressed current C reads:

$$\begin{aligned} \nabla \cdot (\kappa(x) \nabla u(x)) &= \nabla \cdot C, \quad x \in \Omega, \\ \frac{\partial u}{\partial \nu} &= 0 \quad x \in \partial\Omega, \end{aligned}$$

where the volume Ω represents the head, ν is the external normal vector and κ is the conductivity function. The impressed current is often represented by an electric dipole, $C(x) = q\,\delta(x - r_q)$, where δ is the Dirac distribution, r_q is a fixed point in the brain which represents the dipole location, and q is the dipole moment [27]. Observe that, since a static approximation is considered, the values of $u(x)$ do not depend on time; instead they correspond to a precise instant of the underlaying process.

A simplified geometric model is usually considered where the head is represented by a 3D three-layered sphere. The nested subsets $\Omega_3, \Omega_2 \backslash \Omega_3$ and $\Omega_1 \backslash \Omega_2$ correspond to the brain, skull and scalp, respectively. The location of the dipole $r_q \in \Omega_3$ (see Fig. 1) is in the brain. The function $\kappa(x)$ represents the conductivity of

Figure 1: 3D Three-layered Domain

the tissues involved and is usually considered as a positive piecewise constant function

$$\kappa(x) = \begin{cases} \kappa_3 & x \in \Omega_3, \\ \kappa_2 & x \in \Omega_2 \backslash \Omega_3, \\ \kappa_1 & x \in \Omega_1 \backslash \Omega_2, \\ 0 & x \notin \Omega, \end{cases}$$

Assuming that the potential and its normal derivative multiplied by the conductivity function are continuous across the transition surfaces, the following interface conditions are imposed

$$[u]\Big|_{S_i} = 0 \qquad [\kappa(x)\frac{\partial u}{\partial \nu}]\Big|_{S_i} = 0 \quad i = 2, 3.$$

where $[\cdot]\Big|_{S_i}$ denotes the difference between the values of the functions inside the brackets through the interface surfaces $S_i = \partial\Omega_i, i = 1, .., 3$ that surround the different subsets.
In this framework, the forward problem of EEG consists in finding the electric potential u in the head for a given current source C. Conversely the inverse problem of EEG consists in finding the location r_q of the electric dipole and its moment q, for a given scalp potential u. The remaining parameters of the model $\kappa_1, \kappa_2, \kappa_3$, as well as the radii of the spheres, are supposed to be known. We recall that the values of $u(x)$, $x \in \partial\Omega$, do not depend on time, since they are collected at a precise instant.

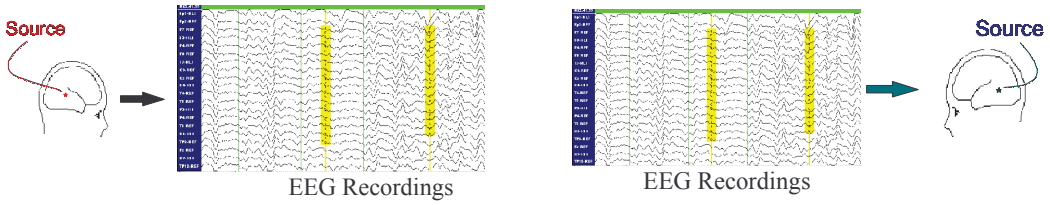

Figure 2: Forward and inverse problems of EEG

Electroencephalographic source localization by noninvasive techniques is an area of interest in clinic epileptology, in particular concerning models of dipolar and distributed sources for the investigation of focal epilepsy. In this context the scalp data corresponding to an instant of a seizure should be considered. An accurate solution to the inverse problem could provide useful information to determine the location of epileptogenic zones within the brain from EEG recordings. In the last decade several authors have been working in this area. Source models were analyzed in [20, 34, 38] while forward and inverse problem solutions were studied in [28, 31, 32], among others. In [16], the authors developed a method for EEG source localization based on rational approximation techniques in the complex plane and they presented results using simulated data. We refer to the references therein for a review of the principal results concerning the inverse problem in EEG.
Since in practice the scalp potential u is measured only at a finite set of points $x_1, \cdots, x_n$, on the scalp where the electrodes are placed, the inverse problem of EEG consists in recovering r_q and q from $u(x_1), \cdots u(x_n)$. Challenged by this problem, we analyze the corresponding mathematical model considering that only a finite set of potential values are available. Parameter estimation techniques and optimal design schemes are performed to solve the inverse problem accurately.

3 Mathematical model

Motivated by the above formulation we consider the following second order elliptic partial differential equation (PDE)

$$\begin{aligned} \nabla \cdot (\kappa(x)\nabla u(x,\theta)) &= \nabla \cdot F(x,\theta), \quad \text{in } \Omega, \\ \frac{\partial u}{\partial \nu}(x,\theta) &= 0 \quad \text{in } \in \partial\Omega, \end{aligned} \tag{5}$$

where Ω is the unit ball of $\mathbb{R}^3$, and κ is a positive piecewise constant function defined by

$$\kappa(x) = \begin{cases} \kappa_3 & x \in \Omega_3, \\ \kappa_2 & x \in \Omega_2 \backslash \Omega_3, \\ \kappa_1 & x \in \Omega_1 \backslash \Omega_2, \\ 0 & x \notin \Omega, \end{cases} \tag{6}$$

where $\Omega_1 = \Omega$ and Ω_2, Ω_3 are balls centered at the origin with radii r_2, r_3 such that $0 < r_3 < r_2 < 1$.

The mathematical formulation is completely defined with the following interface and boundary conditions:

$$[u]\Big|_{S_i} = 0 \qquad [\kappa(x)\frac{\partial u}{\partial \nu}]\Big|_{S_i} = 0 \quad i = 2, 3. \tag{7}$$

$$\frac{\partial u(x)}{\partial \eta} \quad = \quad 0, \qquad x \in \partial G \tag{8}$$

where $[\cdot]_{S_i}$ denotes the difference between the values of the functions inside the brackets through the surface $S_i = \partial\Omega_i$ and η is the external normal vector. This type of system appears in a number of applied problems such electrostatic interrogation systems, medical imaging, geophysical exploration and nondestructive testing, etc, [2, 3, 4, 5, 10, 15, 17, 18, 24, 25, 26, 29, 30].

Once again based on the formulations discussed above, we consider a function F of the form $F(x, \theta) = q\delta(x - r_q)$, where δ denotes the dirac distribution. Then the source $\nabla \cdot F(x, \theta)$ could represent for example an electric dipole with moment $q = (q_1, q_2, q_3) \in \mathbb{R}^3$ and location $r_q = (r_{q_1}, r_{q_2}, r_{q_3}) \in \Omega_3$. The parameter of the model is then $\theta = (r_q, q) \in \mathbb{R}^6$. Existence and uniqueness of a solution $u(x, \theta)$ to this case have been studied in [19] and its dependence with respect to Ω and κ appears in [36, 37], respectively.

In [19] the author gives an explicit formula in terms of a series, for u and its derivatives with respect to the parameters for spherical domains. This formula allows one to compute u at any point of Ω given a dipole that can be located anywhere in Ω. Since we are only interested in computing $u(x)$ for x in the boundary $\partial\Omega$ of the domain and with a dipole located in the innermost layer, i.e., $r_q \in \Omega_3$, we will only recall the expression of u in this situation. The formula for u given in [19] is

$$4\pi u(x) = q \cdot \Big(\frac{r_q}{\|r_q\|}(S_1 - S_0 \cos\omega) + \frac{x}{\|x\|} S_0 \Big), \tag{9}$$

where $\cos\omega = \frac{r_q}{\|r_q\|}\frac{x}{\|x\|}$ is the cosine of the angle formed by the observation point x, the dipole location r_q and the origin, and S_0, S_1 are given by

$$S_0 = \frac{1}{r_0}\sum_{n\geq 1}(2n+1)R_n(r_0, r)P_n'(\cos\omega), \qquad \text{and} \qquad S_1 = \sum_{n\geq 1}(2n+1)R_n'(r_0, r)P_n'(\cos\omega). \tag{10}$$

Here $r_0 = \|r_q\|$, $r = \|x\|$, P_n is the n-th Legendre polynomial and P_n' its derivative which can be computed from the recursive formula

$$P_0(x) = 1,\ P_1(x) = x, \tag{11}$$

$$(n+1)P_{n+1}(x) = (2n+1)xP_n(x) - nP_{n-1}(x), \qquad n \geq 2. \tag{12}$$

Finally, $r_q \in \Omega_3$ implies $r_0 < r_3$, hence the definitions of R_n and R_n' given in [19] reduce to

$$R_n(r_0, r) = -\frac{\{U_3(r_0, 0)\}_{12}}{A} r_0^n, \qquad \text{and} \qquad R_n'(r_0, r) = -\frac{\{U_3(r_0, 0)\}_{22}}{\kappa_3 A} r_0^n,$$

where $A = \{U_1(r_1, r_2)U_2(r_2, r_3)U_3(r_3, 0)\}_{22}$, and the matrix $U_j(r_a, r_b)$ is defined as

$$(2n+1)U_j(r_a, r_b) = \begin{cases} \left(\frac{r_a}{r_b}\right)^{-2n-2} \begin{pmatrix} \frac{nr_a}{r_b} & -\frac{r_a}{\kappa_j} \\ -\frac{n(n+1)\kappa_j}{r_b} & n+1 \end{pmatrix} + \begin{pmatrix} n+1 & \frac{r_b}{\kappa_j} \\ \frac{n(n+1)\kappa_j}{r_a} & \frac{nr_b}{r_a} \end{pmatrix} & \text{if } r_a, r_b \in (r_{j+1}, r_j),\ j = 1, 2 \\ \begin{pmatrix} 0 & \frac{1}{\kappa_3} \\ 0 & \frac{n}{r_a} \end{pmatrix} & \text{if } r_b = 0,\ j = 3. \end{cases} \tag{13}$$

We can thus rewrite R_n and R'_n as

$$R_n(r_0, r) = -\frac{r_0^n}{(2n+1)\kappa_3 A} \qquad \text{and} \qquad R'_n(r_0, r) = -\frac{nr_0^{n-1}}{(2n+1)\kappa_3 A}, \tag{14}$$

so that

$$S_0 = -\frac{1}{\kappa_3}\sum_{n\geq 1}\frac{P'_n(\cos\omega)}{A}r_0^{n-1} \qquad \text{and} \qquad S_1 = -\frac{1}{\kappa_3}\sum_{n\geq 1}\frac{nP'_n(\cos\omega)}{A}r_0^{n-1}. \tag{15}$$

The formula (9) with S_0 and S_1 given by the previous formula (15) allow us to compute easily the solution to (5) when $r_q \in \Omega_3$ and $x \in \partial\Omega$.

4 Inverse problem formulation

We consider the inverse problem or parameter estimation for the mathematical model described by (5). It consists in estimating the unknown parameter $\theta = (r_q, q) \in \mathbb{R}^6$ from the data $y_1, .., y_n$, corresponding to n observation points at $x_1, .., x_n$ on the boundary $\partial\Omega$.

We choose the Ordinary Least Square (OLS) method to calculate estimates $\hat{\theta}$ of θ_0; that is, we minimize

$$J(\theta) = \sum_{j=1}^{n} |u(x_j, \theta) - y_j|^2, \quad \theta \in \mathcal{A}, \tag{16}$$

where $\mathcal{A} = \{(r, q) | r \in \Omega_3\}$. We compute the solution u of our model by means of (9).
The OLS-estimator $\hat{\theta}$ is then

$$\hat{\theta} = \arg\min_{\theta\in\mathcal{A}} J(\theta).$$

Theoretical results concerning existence and ill-posedness of the inverse problem associated with (5)-(8) have been studied in [21, 22, 23].

As already noted, a statistical model is necessary to study and implement inverse problem techniques properly. Here we take the absolute error model (2) with realizations (3). In this context the inverse problem consists of the estimation of the unknown parameters θ_0 from the data

$$y_i := u(x_i, \theta_0) + \epsilon_i \quad , i = 1, .., n,$$

where we assume that the additive noises $\epsilon_1, .., \epsilon_n$ are independent realizations of a centered normal random variable with variance σ^2.

Recall that $\hat{\theta}$ is a realization of a random variable $\hat{\Theta}$. It can be proved that under suitable hypothesis (see [9, 35]), $\hat{\Theta}$ has asymptotically normal distribution

$$\hat{\Theta} \sim N(\theta_0, (\sigma^2 F(x_1, .., x_n, \theta_0))^{-1}), \tag{17}$$

where $F(x_1, .., x_n, \theta) \in \mathbb{R}^{6\times 6}$ is the usual Fisher Information Matrix defined by

$$F_{ij}(x_1, .., x_n, \theta) = \sum_{k=1}^{n} \frac{\partial u}{\partial\theta_i}(x_k, \theta)\frac{\partial u}{\partial\theta_j}(x_k, \theta). \tag{18}$$

The partial derivatives $\frac{\partial u}{\partial \theta_j}(x_k, \theta)$ are the traditional sensitivity functions that, assuming smoothness on u, quantify the variations in u with respect to changes in the j^{th} component of the parameter θ. A precise discussion of the hypothesis and the approximations involved in the above theory is given in [9].

For our model representation, the sensitivities of u with respect to θ can be easily computed by directly differentiating (9). The computation of the derivative $\nabla_q u$ of u with respect to the moment q of the dipole is immediate from (9). For the derivative $\nabla_{r_q} u$ the author in [19] found that

$$\begin{aligned} 4\pi\nabla_{r_q} u(x) &= \frac{r_q}{r_0}\Big\{q\cdot\frac{r_q}{r_0}\Big(\frac{3S_0}{r_0}\cos\omega - \frac{S_1}{r_0} + S_2 - 2S_3\cos\omega + S_4(\cos\omega)^2\Big) + q\cdot x\Big(S_3 - \frac{S_0}{r_0} - S_4\cos\omega\Big)\Big\} \\ &\quad + q\Big\{\frac{S_1}{r_0} - \frac{S_0}{r_0}\cos\omega\Big\} + x\Big\{q\cdot\frac{r_q}{r_0}\Big(S_3 - \frac{S_0}{r_0} - S_4\cos\omega\Big) + q\cdot xS_4\Big\}, \end{aligned} \tag{19}$$

where S_0 and S_1 are given in (15), and S_3, S_4 are defined as

$$S_4 = \frac{1}{r_0^2}\sum_{n\geq 1}(2n+1)R_n(r_0,r)P_n''(\cos\omega) = -\frac{1}{\kappa_3}\sum_{n\geq 1}\frac{P_n''(\cos\omega)}{A}r_0^{n-2},$$

$$S_3 = \frac{1}{r_0}\sum_{n\geq 1}(2n+1)R_n'(r_0,r)P_n'(\cos\omega) = -\frac{1}{\kappa_3}\sum_{n\geq 1}\frac{nP_n'(\cos\omega)}{A}r_0^{n-2}.$$

Here P_n'' is the 2nd derivative of P_n that can be calculated from (11), and one can use the expressions (14) of R_n and R_n' to make the simplifications, and obtain

$$S_2 = \sum_{n\geq 1}(2n+1)R_n''(r_0,r)P_n(\cos\omega).$$

Then using

$$R_n''(r_0,r) = \frac{n(n+1)}{r_0^2}R_n(r_0,r) - \frac{2}{r_0}R_n'(r_0,r) = -\frac{n(n-1)}{(2n+1)\kappa_3 A}r_0^{n-2},$$

we find

$$S_2 = -\frac{1}{\kappa_3}\sum_{n\geq 1}\frac{n(n-1)P_n(\cos\omega)}{A}r_0^{n-2}.$$

4.1 Optimal Design

It is often useful to have some criteria to determine where samples should be taken for any type of interrogation problem, especially those that can be expensive and/or invasive. This is the goal of the optimal design techniques: to search for the *optimal* set of observation points in order to carry on the estimation procedures. Different criteria generally give rise to different selections of observation points. In most cases optimal design methods for parameter estimation problems choose the sampling distribution by minimizing a specific cost function related to the error or to the accuracy in parameter estimates. Data collected in this *optimal* way will lead to parameter estimates with increased accuracy.

In view of the asymptotic distribution (17)-(18) it is natural to choose the points x_i that minimize $F(x_1,..,x_n,\theta_0)$ in some sense (see [6, 7]). A well-known and widely used optimal design method is the D-optimal criteria that consists in minimizing $\det F(x_1,...x_n,\theta)^{-1}$. Geometrically, this corresponds to minimizing the volume of the confidence ellipsoid for the covariance matrix $Cov = \sigma^2 F^{-1}$.

With that purpose we choose the set $\Lambda_D = \{x_{1,D}\ldots, x_{n,D}\} \subset \partial\Omega$ of n observation points where the measurements $\{y_1,...,y_n\}$ are to be obtained by minimizing the function

$$G(x_1,...x_n,\theta_0) = \det F(x_1,...x_n,\theta_0)^{-1}, \quad x_1,...x_n \in \partial\Omega$$

starting with some initial set of points and considering θ_0 as an initial guess value for the parameter. After having selected the observation points, we perform OLS with the optimal set Λ_D and the initial guess θ_0. In the next section we present a detailed description of the way our numerical calculations were performed for the problems of interest to us in this presentation.

5 Numerical Preliminaries

Since we consider simulated data, we are able to study the actual errors and analyze the performance of Optimal Design for an optimal selection of data.

The values used in the numerical simulation are given in the following two tables. Table 1 contains the values for the mathematical model that are used in each numerical experiments. They are fixed values of the model and they are assumed to be known.

Layer	r_i	κ_i
$\Omega_1 \backslash \Omega_2$	1	0.33
$\Omega_2 \backslash \Omega_3$	0.92	0.0042
Ω_3	0.84	0.33

Table 1: Known model values (used for all simulations).

Two different electric dipoles were chosen to illustrate a general behaviour. The first potential dipole (Example 1) is defined by $F(x,y,z) = (3,4,0)\,\delta((x,y,z) - (0.3,0.4,0)))$. It is a *parallel* dipole since its moment $q = (3,4,0)$ is parallel to the vector position $r_q = (0.3,0.4,0)$. The second electric dipole (Example 2) is given by $F(x,y,z) = (2,-1,1)\,\delta((x,y,z) - (0.3,0.4,0)))$. Note that we kept the dipole position while its moment is significantly different. These parameter values and their respective initial relative errors are shown in Table 2.

	Potential Dipole (Case 1)		Potential Dipole (Case 2)	
	Position rq	Moment q	Position rq	Moment q
True Parameter values θ_0	(0.3, 0.4, 0)	(3, 4, 0)	(0.3, 0.4, 0)	(2, -1, 1)
Initial Guess values θ_g	(0.2, 0.2, 0.1)	(2, 2, -1)	(0.1, 0.2, -0.1)	(0, 1, -1)
Initial Relative Error	0.4899	0.8466	0.6000	1.4142

Table 2: Parameter values for inverse problem experiments

The observation data is simulated as

$$y_i = u_i, +\epsilon_i, \qquad i = 1, \ldots, n. \tag{20}$$

where the values $u_i = u(x_i, \theta_0)$, $i = 1, \cdots, n$ are computed as a sum of 20 terms of the form given in (9), for $\theta_0 = (0.3,\ 0.4,\ 0,\ 3,\ 4,\ 0)$ in the first example and $\theta_0 = (0.3,\ 0.4,\ 0,\ 2,\ -1,\ 1)$ in the second.

The observation noise ϵ_i at each observation point x_i is calculated by the Matlab function **randn** with standard deviations $\sigma = 0,\ 0.05,\ 0.1,\ 0.15$ and 0.2 to produce noise free data as well as data sets with nontrivial increasing noise levels.

Note that the observation data is taken for the outer surface of the domain which is considered as a unit sphere ($r_3 = 1$). Hence, the observation points can be written as $(x,y,z) = (\sin(\alpha)\cos(\phi), \sin(\alpha)\sin(\phi), \cos(\alpha))$, with $(\alpha,\phi) \in [0,\pi] \times [0,2\pi]$. We define a uniform grid on spherical coordinates with constant step $\Delta\alpha = \pi/30$ for α and $\Delta\phi = 2 * \pi/30$ for ϕ. This gives us 31×31 grid points in the rectangle $[0,\pi] \times [0,2\pi]$ of the form

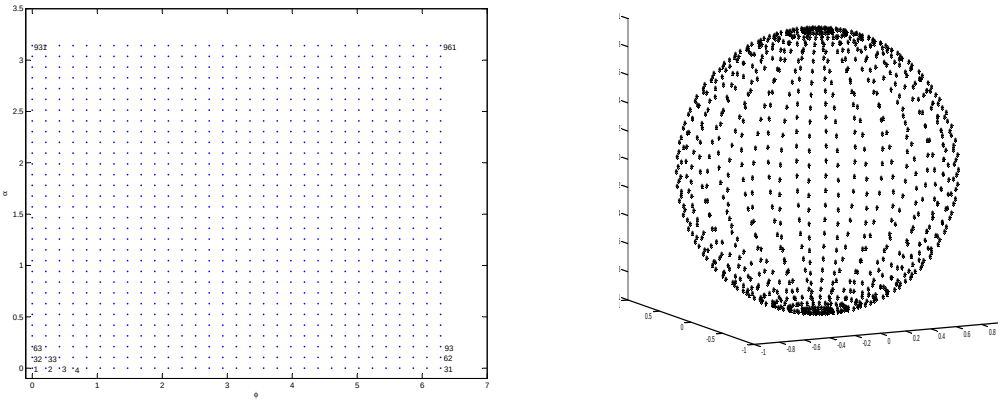

Figure 3: Rectangular grid in (ϕ, α) (left) and Spherical grid (right).

(α_i, ϕ_j) where $\alpha_i = (i-1) * \Delta\alpha$, $i = 1, ..., 31$, $\phi_j = (j-1) * \Delta\phi$, $j = 1, ..., 31$. The gridpoints are numbered on the rectangular grid from left to right and from bottom to top as shown in Fig. 3 (left). The spherical gridpoints are shown in Fig. 3, on the right. Note that the bottom line of gridpoints correspond to $\alpha = 0$ and the top line to $\alpha = \phi$. Each of these lines correspond to only one point on the unit sphere, they are $(0, 0, 1)$ and $(0, 0, -1)$ in cartesian coordinates, which are the *poles*. On the other hand, the extreme points of the same line are the same, due to the periodicity of trigonometrical functions. One needs to take these facts into account when considering observation points.

As mentioned before, the estimated value for the parameter is based on the initial set Λ of observation points.

We ran numerical experiments considering different numbers of measurements from $n = 7$ to $n = 20$. For each case, the points x_i, $i = 1, .., n$ in Λ are chosen from the set of *observable* gridpoints as follows. First, we fix the first and the last points of Λ at the gridpoints numbered as 100 and 650, respectively; that is $x_1 = xg_{100}$, $x_n = xg_{650}$. In this way we are sure that they fall far from the poles. The rest of the points are *uniformly* distributed on the numbered grid, which means

$$x_l = xg_k, \quad k = 100 + (l-1)\frac{550}{n-1}, \quad l = 1, ..., n. \tag{21}$$

6 Parameter estimation

We obtain two estimates $\hat{\theta}_\Lambda$ and $\hat{\theta}_D$ of θ_0 performing OLS with the initial guess θ_g and two different sets of observations points $x_1, \ldots, x_n$:

- the estimate $\hat{\theta}_\Lambda$ is obtained performing OLS with the initial guess θ_g and the set $\Lambda = \{\tilde{x}_1, \ldots, \tilde{x}_n\}$ of observation points given by (21).

- we obtain a second estimate $\hat{\theta}_D$ of θ_0 applying OLS using the observation points arising from the D-optimal design criteria as follows. We first look for a set $\Lambda_D = \{x_1^D, \ldots, x_n^D\}$ of n observation points minimizing the function

$$\det F(x_1, ...x_n, \theta_g)^{-1}$$

starting with Λ as initial observation points. We then perform OLS with θ_g as initial guess for θ and the observation points in Λ_D .

The D-optimal set of observations points are calculated by means of the Matlab function **fmincon** with the following *optimset*: MaxIter=50000,MaxFunEvals=700000,TolFun=1e-21,TolX=1e-6, with constraints 0, π for α and 0, 2π for ϕ.

The OLS-estimate is computed by the Matlab function **lsqnonlin** with the same options as **fmincon** except that in this case we set TolFun=1e-10.

We repeat these procedures N times (generating a new set of perturbations $\epsilon_1, , \epsilon_n$ each time) thus we obtain $2N$ different estimates: N of them denoted by $\theta^j_\Lambda = (\hat{r}^j_{q\Lambda}, \hat{q}^j_\Lambda)$, $j = 1, \ldots, N$ (OLS estimates) and the remaining ones denoted by $\theta^j_D = (\hat{r}^j_{qD}, \hat{q}^j_D)$, $j = 1, \ldots, N$ (D-Optimal -OLS estimates). We then compute the relatives errors for r_q and q:

$$e^j_\Lambda(r_q) := \frac{\|\hat{r_q}^j_\Lambda - r_{q_0}\|}{\|r_{q_0}\|}, \qquad e^j_\Lambda(q) := \frac{\|\hat{q}^j_\Lambda - q_0\|}{\|q_0\|}, j = 1, .., N,$$

$$e^j_D(r_q) := \frac{\|\hat{r_q}^j_D - r_{q_0}\|}{\|r_{q_0}\|}, \qquad e^j_D(q) := \frac{\|\hat{q}^j_D - q_0\|}{\|q_0\|}, i = j, .., N,$$

and then average them:

$$\bar{e}_\Lambda(r_q) = \frac{1}{N}\sum_{j=1}^{N} e^j_\Lambda(r_q), \qquad \bar{e}_D(r_q) = \frac{1}{N}\sum_{j=1}^{N} e^j_D(r_q), \tag{22}$$

$$\bar{e}_\Lambda(q) = \frac{1}{N}\sum_{j=1}^{N} e^j_\Lambda(q), \qquad \bar{e}_D(q) = \frac{1}{N}\sum_{j=1}^{N} e^j_D(q). \tag{23}$$

6.1 Example 1: (parallel dipole)

We first consider a parallel dipole where the "true" values for the parameters are given by

$$\theta_0 = (0.3,\ 0.4,\ 0,\ 3,\ 4,\ 0)$$

and the initial "guess" values are

$$\theta_g = (0.2,\ 0.2,\ 0.1,\ 2,\ 2,\ -1).$$

Tables 3 and 4 give the resulting values for $\bar{e}_\Lambda(r_q)$, $\bar{e}_D(r_q)$, and for $\bar{e}_\Lambda(q)$, $\bar{e}_D(q)$, respectively, for $N = 500$ with $n = 7, \ldots, 20$ observation points and noise standard deviations $\sigma = 0,\ 0.05,\ 0.1,\ 0.15,\ 0.2$ for Example 1 (the parallel dipole example). These values are displayed graphically in Figures 4 (No optimal design) and 5 (D-optimal design).

We denote by $\hat{\theta}_\Lambda = (\hat{rq}_\Lambda, \hat{q}_\Lambda)$ and $\hat{\theta}_D = (\hat{rq}_D, \hat{q}_D)$ the average of the estimated parameters $\{\hat{\theta}^j_\Lambda\}_{1\le j\le N}$ and $\{\hat{\theta}^j_D\}_{1\le j\le N}$, namely

$$\hat{\theta}_\Lambda = \frac{1}{N}\sum_{i=1}^{N} \hat{\theta}^i_\Lambda, \qquad \hat{\theta}_D = \frac{1}{N}\sum_{i=1}^{N} \hat{\theta}^i_D.$$

To compare the statistical relevance of $\hat{\theta}_\Lambda$ and $\hat{\theta}_D$ we compute the confidence intervals (CI) for θ_0 based on these two estimates in the following way. We first generate two sets of simulated observations $\{u_{i,D}\}_{1\le i\le n}$

$n\backslash\sigma$	$\sigma = 0.2$		$\sigma = 0.15$		$\sigma = 0.1$		$\sigma = 0.05$		$\sigma = 0$	
n	$\bar{e}_D(r_q)$	$\bar{e}_\Lambda(r_q)$	$\bar{e}_D(r_q)$	$\bar{e}_\Lambda(r_q)$	$\bar{e}_D(r_q)$	$\bar{e}_\Lambda(r_q)$	$\bar{e}_D(r_q)$	$\bar{e}_\Lambda(r_q)$	$\bar{e}_D(r_q)$	$\bar{e}_\Lambda(r_q)$
7	0.2855	1.1511	0.2053	1.0705	0.1299	0.8931	0.0654	0.6581	0.65e-15	0.49e-11
8	0.2079	0.6825	0.1549	0.5100	0.0995	0.3342	0.0498	0.1671	0.47e-12	0.76e-11
9	0.2024	0.4586	0.1535	0.3454	0.1017	0.2370	0.0493	0.1121	0.16e-14	0.11e-14
10	0.1990	1.2967	0.1362	1.1389	0.0931	0.9728	0.0453	0.5965	0.10e-12	0.61e-12
11	0.1946	0.3172	0.1453	0.2392	0.0958	0.1481	0.0467	0.0728	0.27e-15	0.77e-15
12	0.1790	0.3753	0.1328	0.2595	0.0845	0.1649	0.0404	0.0821	0.74e-15	0.54e-13
13	0.1837	0.3752	0.1297	0.2846	0.0896	0.1863	0.0432	0.0951	0.60e-14	0.20e-12
14	0.1636	0.3295	0.1213	0.2175	0.0793	0.1375	0.0400	0.0722	0.25e-14	0.20e-12
15	0.1601	0.2622	0.1232	0.1996	0.0793	0.1294	0.0402	0.0629	0.14e-14	0.56e-14
16	0.1521	0.2581	0.1181	0.1865	0.0744	0.1252	0.0384	0.0603	0.41e-15	0.77e-15
17	0.1546	0.2990	0.1153	0.2133	0.0732	0.1385	0.0371	0.0676	0.34e-15	0.90e-15
18	0.1489	1.0426	0.1091	0.9104	0.0727	0.7076	0.0373	0.4087	0.16e-15	0.38e-13
19	0.1481	0.8855	0.1063	0.7488	0.0720	0.6297	0.0355	0.4026	0.48e-12	0.13e-10
20	0.1360	0.2067	0.1019	0.1477	0.0695	0.1024	0.0350	0.0494	0.12e-15	0.36e-15

Table 3: Example 1. Mean relative errors $\bar{e}_D(r_q)$ and $\bar{e}_\Lambda(r_q)$ for r_q as defined in (22) for different number of observation points n and different value of the noise standard deviation σ.

$n\backslash\sigma$	$\sigma = 0.2$		$\sigma = 0.15$		$\sigma = 0.1$		$\sigma = 0.05$		$\sigma = 0$	
n	$\bar{e}_D(r_q)$	$\bar{e}_\Lambda(r_q)$	$\bar{e}_D(r_q)$	$\bar{e}_\Lambda(r_q)$	$\bar{e}_D(r_q)$	$\bar{e}_\Lambda(r_q)$	$\bar{e}_D(r_q)$	$\bar{e}_\Lambda(r_q)$	$\bar{e}_D(r_q)$	$\bar{e}_\Lambda(r_q)$
7	0.1151	0.7379	0.0861	0.6432	0.0591	0.4887	0.0289	0.3058	0.17e-15	0.19e-11
8	0.1033	0.2099	0.0769	0.1509	0.0512	0.1013	0.0264	0.0497	0.07e-12	0.21e-11
9	0.1030	0.1285	0.0788	0.0947	0.0523	0.0638	0.0252	0.0307	0.02e-14	0.06e-14
10	0.0986	0.7908	0.0709	0.6081	0.0485	0.4683	0.0239	0.2570	0.04e-12	0.51e-12
11	0.0921	0.0825	0.0741	0.0677	0.0481	0.0425	0.0235	0.0216	0.28e-15	0.09e-15
12	0.0919	0.0963	0.0658	0.0678	0.0444	0.0448	0.0215	0.0218	0.16e-15	0.15e-13
13	0.0862	0.1717	0.0630	0.1197	0.0435	0.0837	0.0219	0.0412	0.08e-14	0.12e-12
14	0.0807	0.0834	0.0617	0.0586	0.0400	0.0387	0.0207	0.0192	0.01e-14	0.05e-11
15	0.0779	0.0783	0.0585	0.0565	0.0396	0.0376	0.0205	0.0183	0.01e-14	0.16e-14
16	0.0786	0.0761	0.0600	0.0562	0.0390	0.0370	0.0204	0.0177	0.09e-15	0.10e-15
17	0.0765	0.0900	0.0572	0.0647	0.0375	0.0422	0.0192	0.0213	0.00e-15	0.40e-15
18	0.0744	0.2039	0.0571	0.1697	0.0374	0.1323	0.0185	0.0714	0.25e-15	0.12e-13
19	0.0714	0.5487	0.0559	0.4251	0.0368	0.3129	0.0178	0.1762	0.15e-12	0.02e-10
20	0.0706	0.0741	0.0519	0.0538	0.0345	0.0357	0.0183	0.0183	0.14e-15	0.03e-15

Table 4: Example 1. Mean relative errors $\bar{e}_D(q)$ and $\bar{e}_\Lambda(q)$ for q as defined in (23) for different number of observation points n and different value of the noise standard deviation σ.

and $\{u_{i,\Lambda}\}_{1\le i\le n}$ defined in (20) using the set of observation points Λ_D and Λ respectively. We then compute the estimated variances $\hat{\sigma}^2_\Lambda$ and $\hat{\sigma}^2_D$ defined as

$$\hat{\sigma}^2_\Lambda = \frac{1}{n-6}\sum_{i=1}^{n}\Big(u_{i,\Lambda} - u(\tilde{x}_i, \hat{\theta}_\Lambda)\Big)^2, \qquad \hat{\sigma}^2_D = \frac{1}{n-6}\sum_{i=1}^{n}\Big(u_{i,D} - u(x_i^D, \hat{\theta}_D)\Big)^2.$$

The standard errors $SE(\hat{\theta}_\Lambda)$, $SE(\hat{\theta}_D) \in \mathbb{R}^6$ are then defined as

$$SE_k^2(\hat{\theta}_\Lambda) = \hat{\sigma}_\Lambda^2 (F(\tilde{x}_1, \ldots, \tilde{x}_n; \hat{\theta}_\Lambda)^{-1})_{kk}, \qquad SE_k^2(\hat{\theta}_D) = \hat{\sigma}_D^2 (F(x_1^D, \ldots, x_n^D; \hat{\theta}_D)^{-1})_{kk}$$

where $k = 1, \ldots, 6$, and F is the Fisher matrix defined in (18). The approximate CI at the $(1-\alpha)\%$ level for the k-th component $\theta_{0,k}$ of θ_0 corresponding to $\hat{\theta}_\Lambda$ and $\hat{\theta}_D$ are then given respectively by

$$[\,\hat{\theta}_{\Lambda,k} \,-\, t_{1-\alpha/2}\, SE_k(\hat{\theta}_\Lambda)\,,\, \hat{\theta}_{\Lambda,k} \,+\, t_{1-\alpha/2}\, SE_k(\hat{\theta}_\Lambda)\,] \tag{24}$$

$$[\,\hat{\theta}_{D,k} \,-\, t_{1-\alpha/2}\, SE_k(\hat{\theta}_D)\,,\, \hat{\theta}_{D,k} \,+\, t_{1-\alpha/2}\, SE_k(\hat{\theta}_D)\,]. \tag{25}$$

The results for $r_q(1)$ (the first component of r_q) and $q(1)$ (the first component of q) are shown in Figures (6)-(9). Figure 6 depicts the results when $\sigma = 0.05$. From top to bottom: The mean relative errors, length of the confidence intervals (built using formula (24) (in blue) and (25)) and the confidence intervals. On the left are the results for $r_q(1)$ and on the right are the results for $q(1)$. Similar results for $\sigma = 0.1, 0.15, 0.2$ are depicted in Figures 7 - 9.

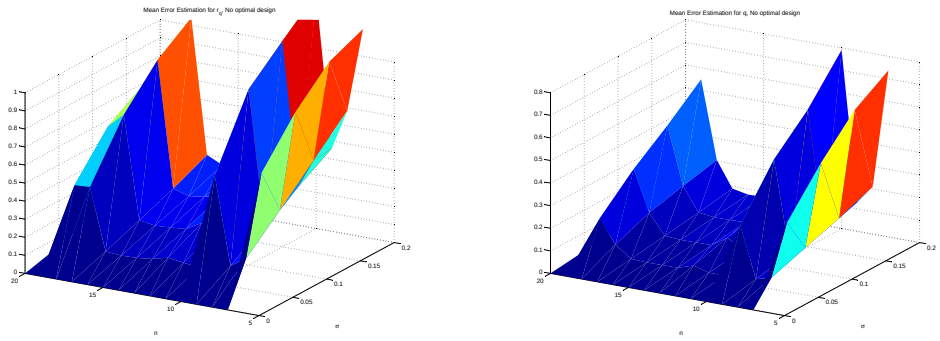

Figure 4: Mean relative errors $\bar{e}_\Lambda(r_q)$ and $\bar{e}_\Lambda(q)$ (no optimal design) as functions of n and σ .

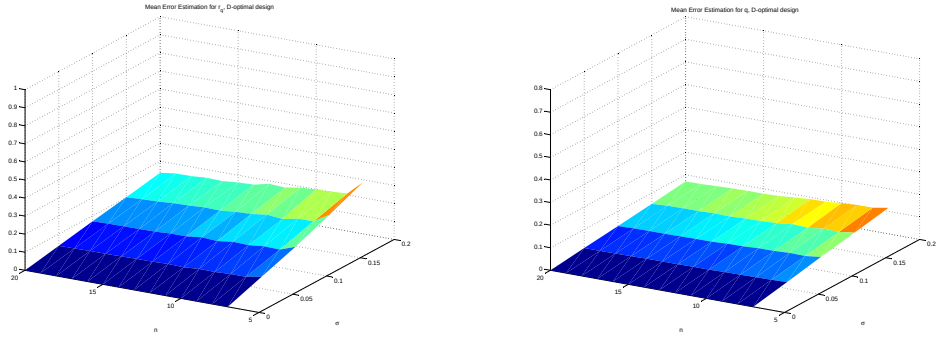

Figure 5: Mean relative errors $\bar{e}_D(r_q)$ and $\bar{e}_D(q)$ (using D-Optimal design) as functions of n and σ.

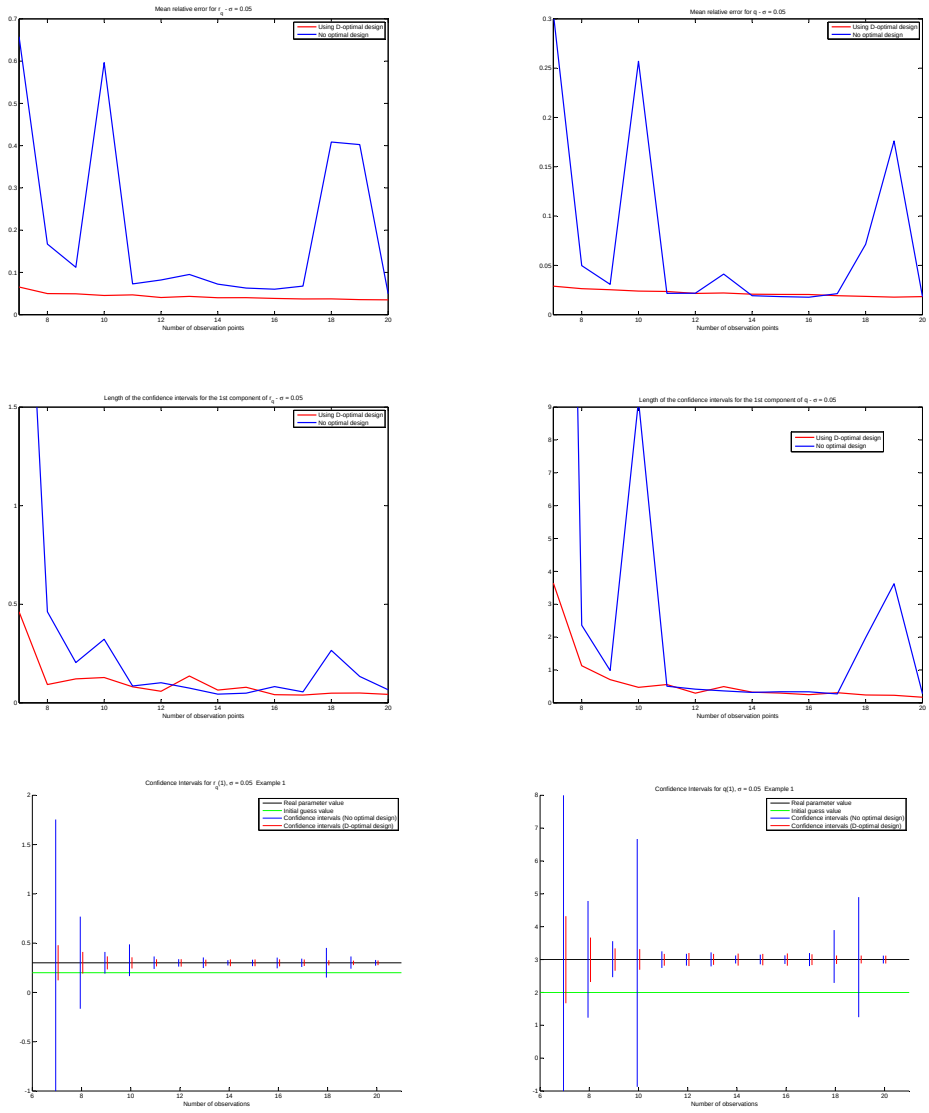

Figure 6: Results for noisy realizations with $\sigma = 0.05$ using D-optimal design (red) and no optimal design (blue). From top to bottom: Mean relative errors $\bar{e}_D(r_q)$ and $\bar{e}_\Lambda(r_q)$ (right) and $\bar{e}_D(q)$ and $\bar{e}_\Lambda(q)$ (left); length of confidence intervals for $r_q(1)$ (right) and $q(1)$ (left); confidence intervals at 90 % confidence level for $r_q(1)$ (right) and $q(1)$ (left).

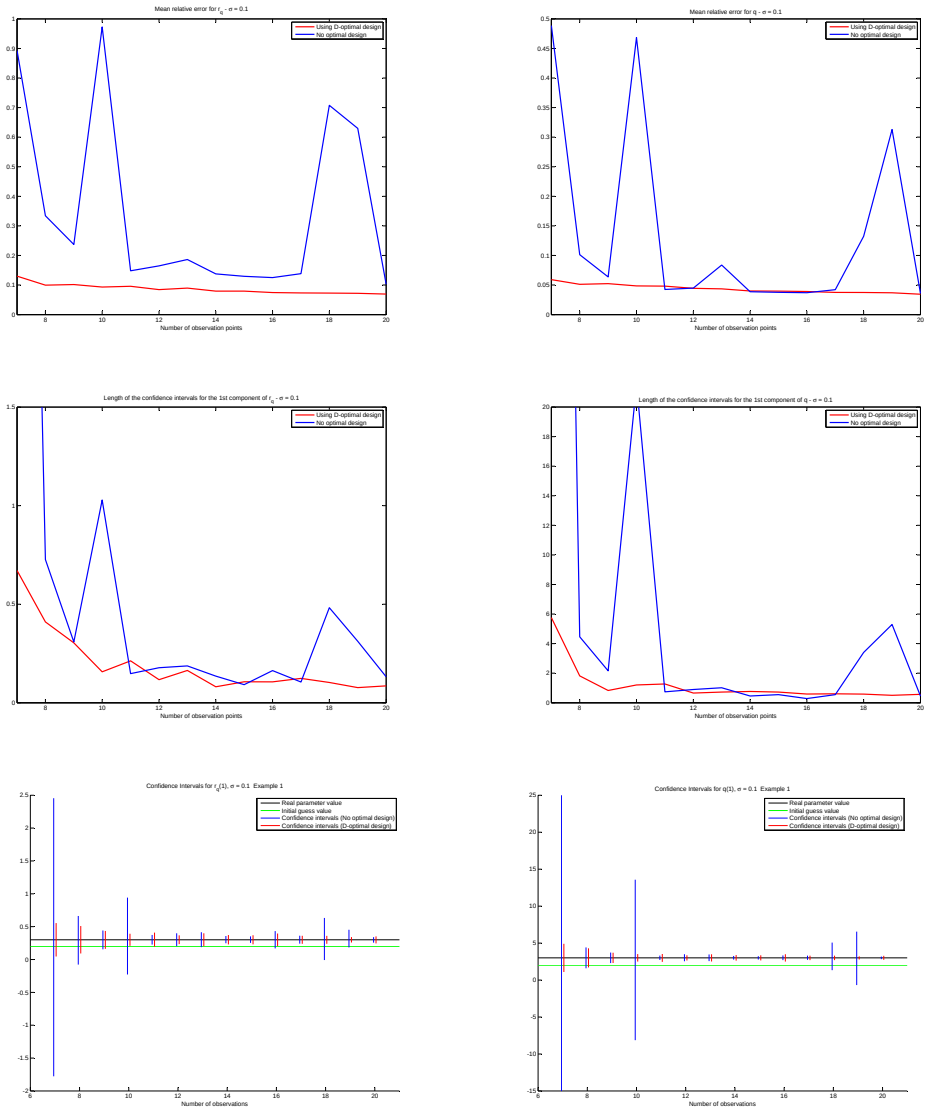

Figure 7: Results for noisy realizations with $\sigma = 0.1$ using D-optimal design (red) and no optimal design (blue). From top to bottom: Mean relative errors $\bar{e}_D(r_q)$ and $\bar{e}_\Lambda(r_q)$ (right) and $\bar{e}_D(q)$ and $\bar{e}_\Lambda(q)$ (left); length of confidence intervals for $r_q(1)$ (right) and $q(1)$ (left); confidence intervals at 90 % confidence level for $r_q(1)$ (right) and $q(1)$ (left).

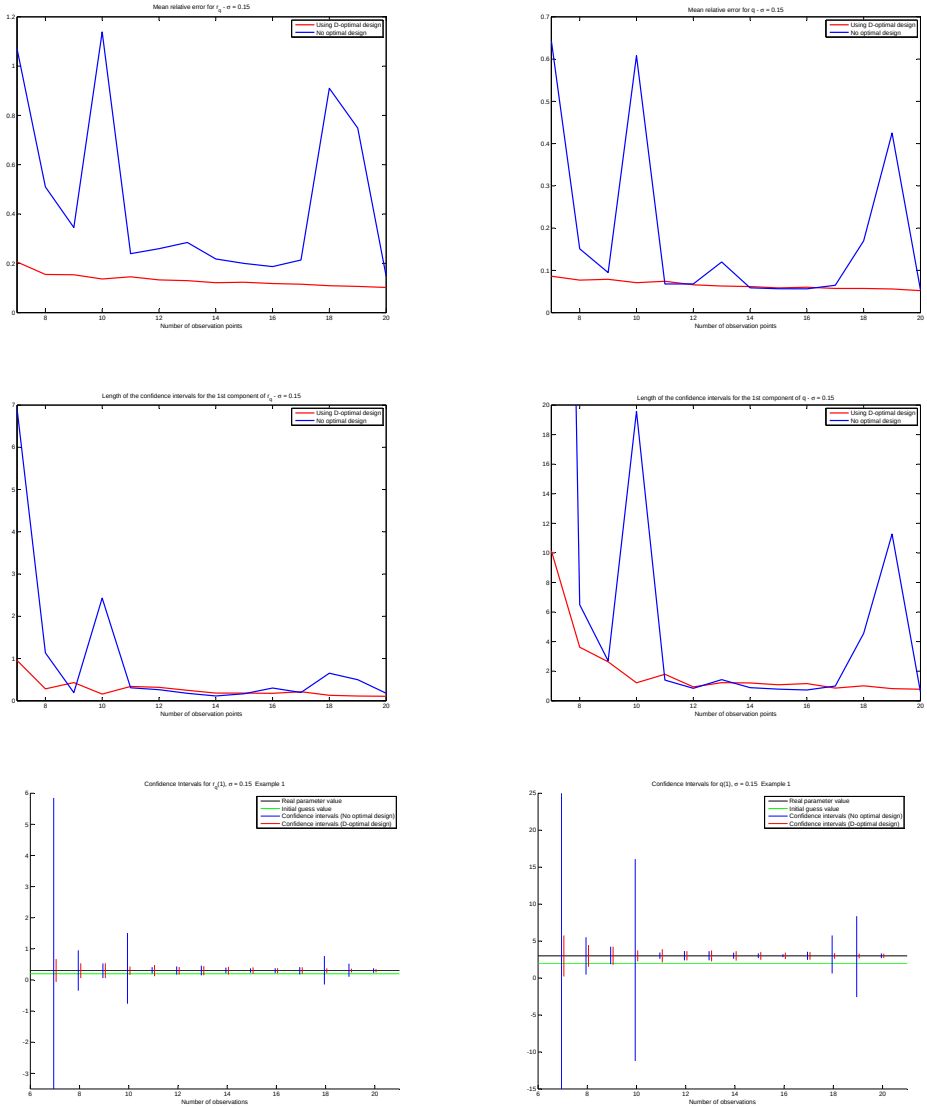

Figure 8: Results for noisy realizations with $\sigma = 0.15$ using D-optimal design (red) and no optimal design (blue). From top to bottom: Mean relative errors $\bar{e}_D(r_q)$ and $\bar{e}_\Lambda(r_q)$ (right) and $\bar{e}_D(q)$ and $\bar{e}_\Lambda(q)$ (left); length of confidence intervals for $r_q(1)$ (right) and $q(1)$ (left); confidence intervals at 90 % confidence level for $r_q(1)$ (right) and $q(1)$ (left).

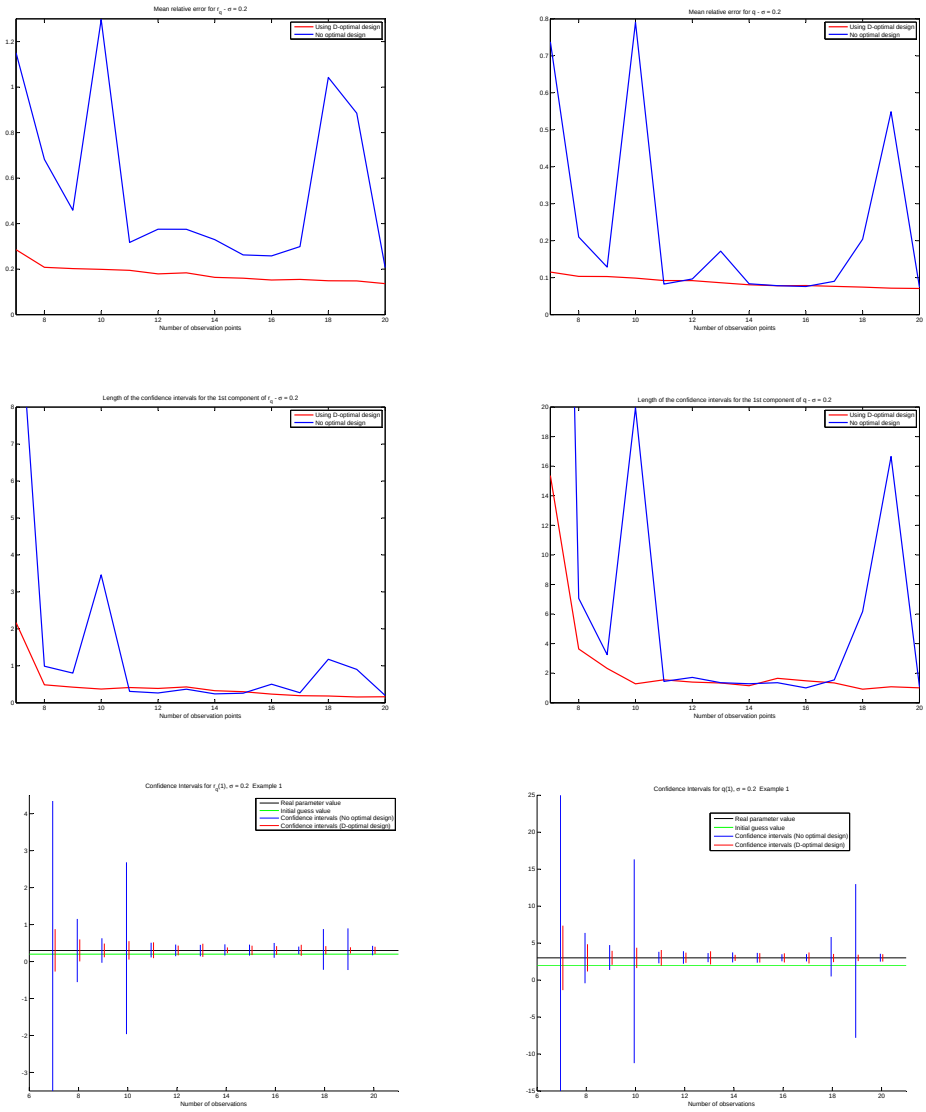

Figure 9: Results for noisy realizations with $\sigma = 0.2$ using D-optimal design (red) and no optimal design (blue). From top to bottom: Mean relative errors $\bar{e}_D(r_q)$ and $\bar{e}_\Lambda(r_q)$ (right) and $\bar{e}_D(q)$ and $\bar{e}_\Lambda(q)$ (left); length of confidence intervals for $r_q(1)$ (right) and $q(1)$ (left); confidence intervals at 90 % confidence level for $r_q(1)$ (right) and $q(1)$ (left).

6.2 Example 2: (nonparallel dipole)

To illustrate our findings with a second example, we consider Example 2 introduced above where the moment and location are *non parallel*. In this case we chose true values for $\theta_0 = (0.3,\ 0.4,\ 0,\ 2,\ -1,\ 1)$ and used initial guess parameter values $\theta_g = (0.1,\ 0.2, \text{-}0.1,\ 0,\ 1,\ \text{-}1)$. Results for different levels of noise are given in Tables 5 and 6. Findings for mean relative errors and confidence intervals of level 90 % are given in Figures 12 - 15.

$n\backslash\sigma$	$\sigma = 0.2$		$\sigma = 0.15$		$\sigma = 0.1$		$\sigma = 0.05$		$\sigma = 0$	
n	$\bar{e}_D(r_q)$	$\bar{e}_\Lambda(r_q)$	$\bar{e}_D(r_q)$	$\bar{e}_\Lambda(r_q)$	$\bar{e}_D(r_q)$	$\bar{e}_\Lambda(r_q)$	$\bar{e}_D(r_q)$	$\bar{e}_\Lambda(r_q)$	$\bar{e}_D(r_q)$	$\bar{e}_\Lambda(r_q)$
7	0.6689	1.6881	0.5211	1.6300	0.3268	1.6121	0.1615	1.4561	0.77e-015	1.8753
8	0.6009	1.2706	0.4581	1.2127	0.2975	1.0428	0.1480	0.6399	0.51e-015	0.70e-13
9	0.4500	0.6348	0.3317	0.4826	0.2133	0.3018	0.1061	0.1496	0.81e-015	0.28e-15
10	0.4272	1.5717	0.3194	1.4599	0.2005	1.2102	0.0951	0.6284	0.23e-13	0.56e-13
11	0.3774	0.5114	0.2665	0.1378	0.1790	0.2730	0.0886	0.1257	0.79e-15	0.26e-15
12	0.4544	0.4597	0.3227	0.3693	0.2077	0.2291	0.1082	0.1103	0.12e-14	0.85e-15
13	0.3573	0.9601	0.2855	0.7718	0.1748	0.5196	0.0898	0.2374	0.14e-13	0.47e-10
14	0.3666	0.4256	0.2572	0.3180	0.1653	0.2064	0.0833	0.1004	0.17e-14	0.40e-15
15	0.3891	0.4339	0.2700	0.3063	0.1865	0.2006	0.0890	0.0998	0.73e-12	0.47e-12
16	0.3235	0.4291	0.2384	0.3217	0.1589	0.2043	0.0766	0.0983	0.30e-14	0.65e-15
17	0.3107	0.4009	0.2277	0.3129	0.1559	0.1928	0.0758	0.0988	0.17e-13	0.11e-13
18	0.3306	1.079	0.2494	0.8558	0.1645	0.6944	0.0779	0.4231	0.49e-15	0.36e-10
19	0.3067	1.225	0.2317	1.0808	0.1562	0.7549	0.0783	0.3312	0.33e-15	0.34e-14
20	0.2957	0.444	0.2294	0.3061	0.1429	0.2042	0.0719	0.0976	0.14e-15	0.38e-11

Table 5: Example 2. Mean relative errors $\bar{e}_D(q)$ and $\bar{e}_\Lambda(q)$ for q as defined in (22) for different number of observation points n and different value of the noise standard deviation σ.

$n\backslash\sigma$	$\sigma = 0.2$		$\sigma = 0.15$		$\sigma = 0.1$		$\sigma = 0.05$		$\sigma = 0$	
n	$\bar{e}_D(q)$	$\bar{e}_\Lambda(q)$	$\bar{e}_D(q)$	$\bar{e}_\Lambda(q)$	$\bar{e}_D(q)$	$\bar{e}_\Lambda(q)$	$\bar{e}_D(q)$	$\bar{e}_\Lambda(q)$	$\bar{e}_D(q)$	$\bar{e}_\Lambda(q)$
7	0.2550	1.4185	0.1861	1.3604	0.1156	1.3236	0.0544	1.1651	0.25e-15	1.2367
8	0.2319	0.6808	0.1727	0.6256	0.1073	0.4962	0.0513	0.2662	0.27e-15	0.29e-13
9	0.2013	0.2316	0.1573	0.1705	0.0961	0.1140	0.0495	0.0577	0.15e-15	0.04e-15
10	0.2007	1.233	0.1482	1.0346	0.0902	0.8368	0.0448	0.3594	0.04e-13	0.42e-13
11	0.1844	0.1843	0.1311	0.1378	0.0902	0.0900	0.0409	0.0437	0.24e-15	0.22e-15
12	0.1920	0.1851	0.1351	0.1435	0.0851	0.0912	0.0447	0.0459	0.04e-14	0.22e-15
13	0.1648	0.5212	0.1246	0.4082	0.0795	0.2526	0.0396	0.1057	0.05e-13	0.16e-10
14	0.1516	0.1628	0.1107	0.1211	0.0728	0.0803	0.0360	0.0377	0.02e-14	0.00e-15
15	0.1644	0.1713	0.1202	0.1244	0.0806	0.0824	0.0388	0.0410	0.27e-12	0.16e-12
16	0.1416	0.1477	0.1087	0.1155	0.0683	0.0724	0.0358	0.0378	0.13e-14	0.29e-15
17	0.1459	0.1484	0.1088	0.1121	0.0715	0.0718	0.0349	0.0359	0.01e-13	0.00e-13
18	0.1441	0.322	0.1045	0.2434	0.0680	0.1924	0.0333	0.1198	0.10e-15	0.18e-10
19	0.1296	0.944	0.0993	0.7791	0.0656	0.5600	0.0344	0.2457	0.16e-15	0.54e-14
20	0.1299	0.197	0.0984	0.1377	0.0641	0.0917	0.0321	0.0441	0.20e-15	0.15 e-11

Table 6: Example 2. Mean relative errors $\bar{e}_D(q)$ and $\bar{e}_\Lambda(q)$ for q as defined in (23) for different number of observation points n and different value of the noise standard deviation σ.

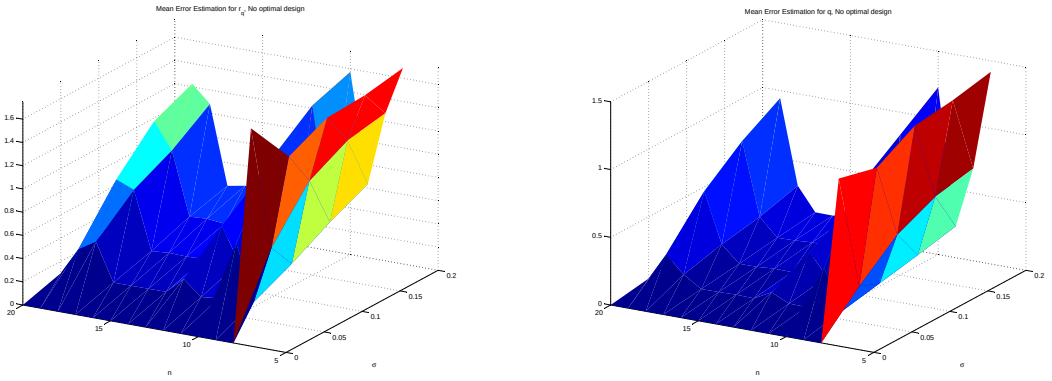

Figure 10: Mean relative errors $\bar{e}_\Lambda(r_q)$ and $\bar{e}_\Lambda(q)$ (no optimal design) as functions of n and σ.

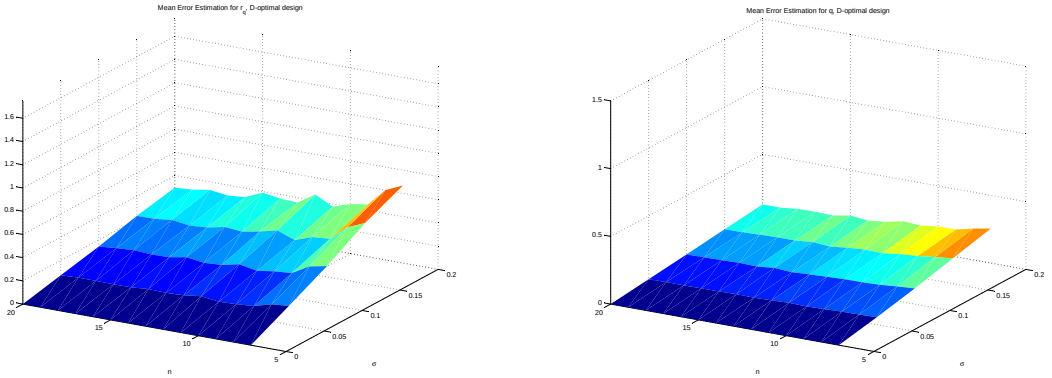

Figure 11: Mean relative errors $\bar{e}_D(r_q)$ and $\bar{e}_D(q)$ (using D-optimal design) as functions of n and σ.

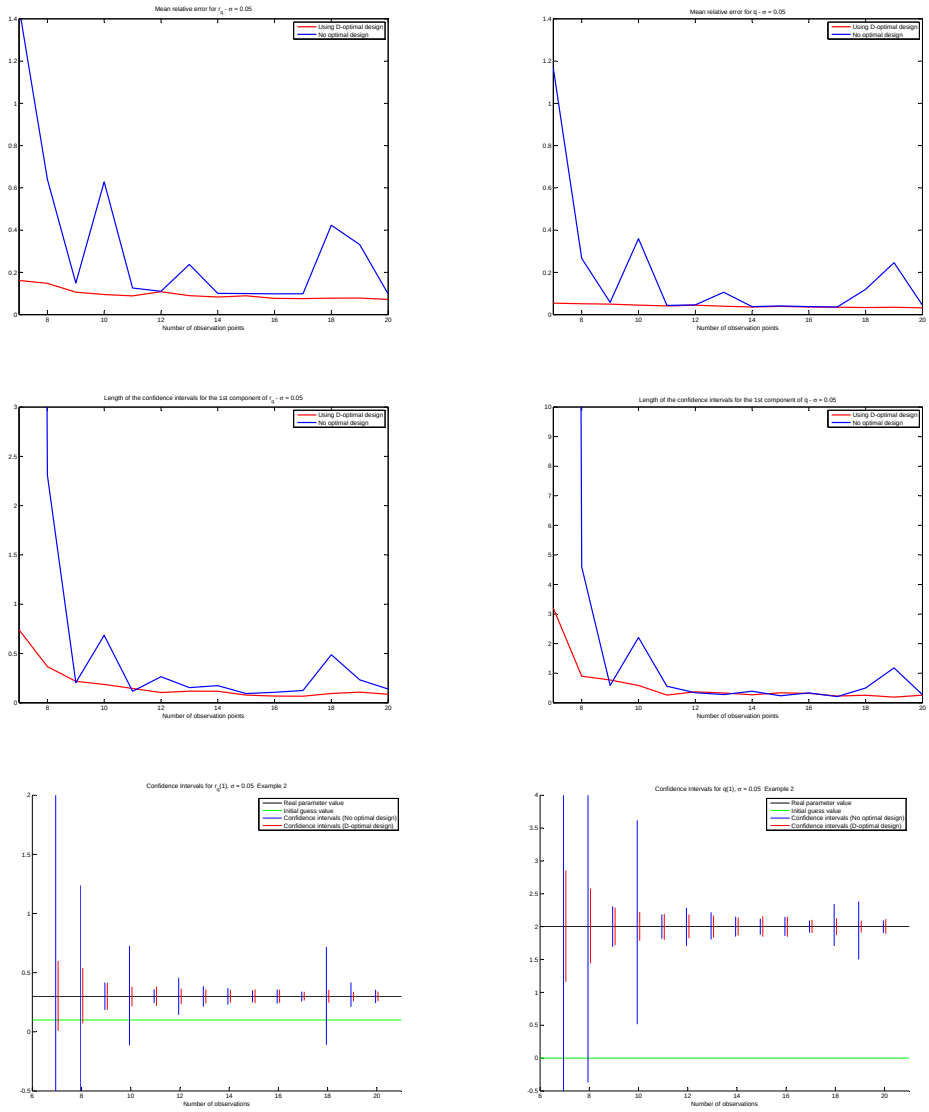

Figure 12: Results for noisy realizations with $\sigma = 0.05$ using D-optimal design (red) and no optimal design (blue). From top to bottom: Mean relative errors $\bar{e}_D(r_q)$ and $\bar{e}_\Lambda(r_q)$ (right) and $\bar{e}_D(q)$ and $\bar{e}_\Lambda(q)$ (left); length of confidence intervals for $r_q(1)$ (right) and $q(1)$ (left); confidence intervals at 90 % confidence level for $r_q(1)$ (right) and $q(1)$ (left).

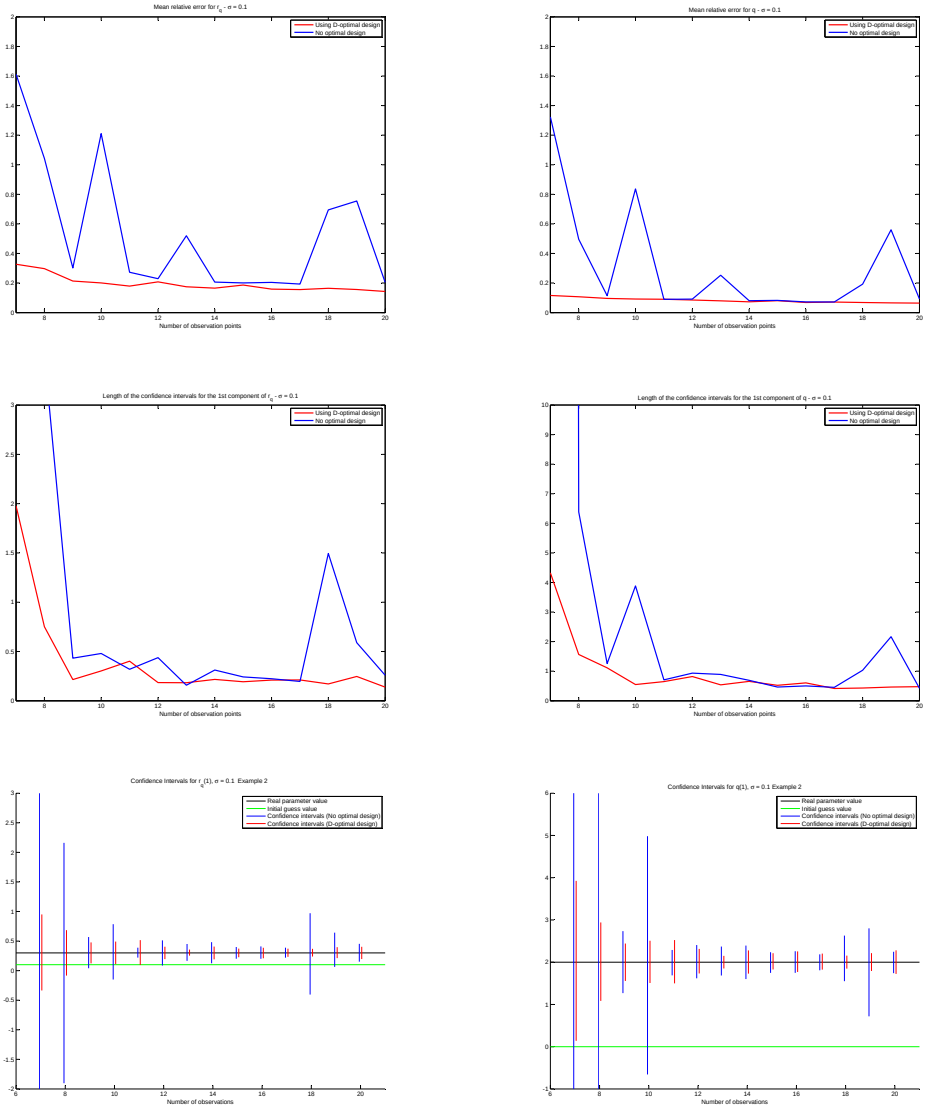

Figure 13: Results for noisy realizations with $\sigma = 0.1$ using D-optimal design (red) and no optimal design (blue). From top to bottom: Mean relative errors $\bar{e}_D(r_q)$ and $\bar{e}_\Lambda(r_q)$ (right) and $\bar{e}_D(q)$ and $\bar{e}_\Lambda(q)$ (left); length of confidence intervals for $r_q(1)$ (right) and $q(1)$ (left); confidence intervals at 90 % confidence level for $r_q(1)$ (right) and $q(1)$ (left).

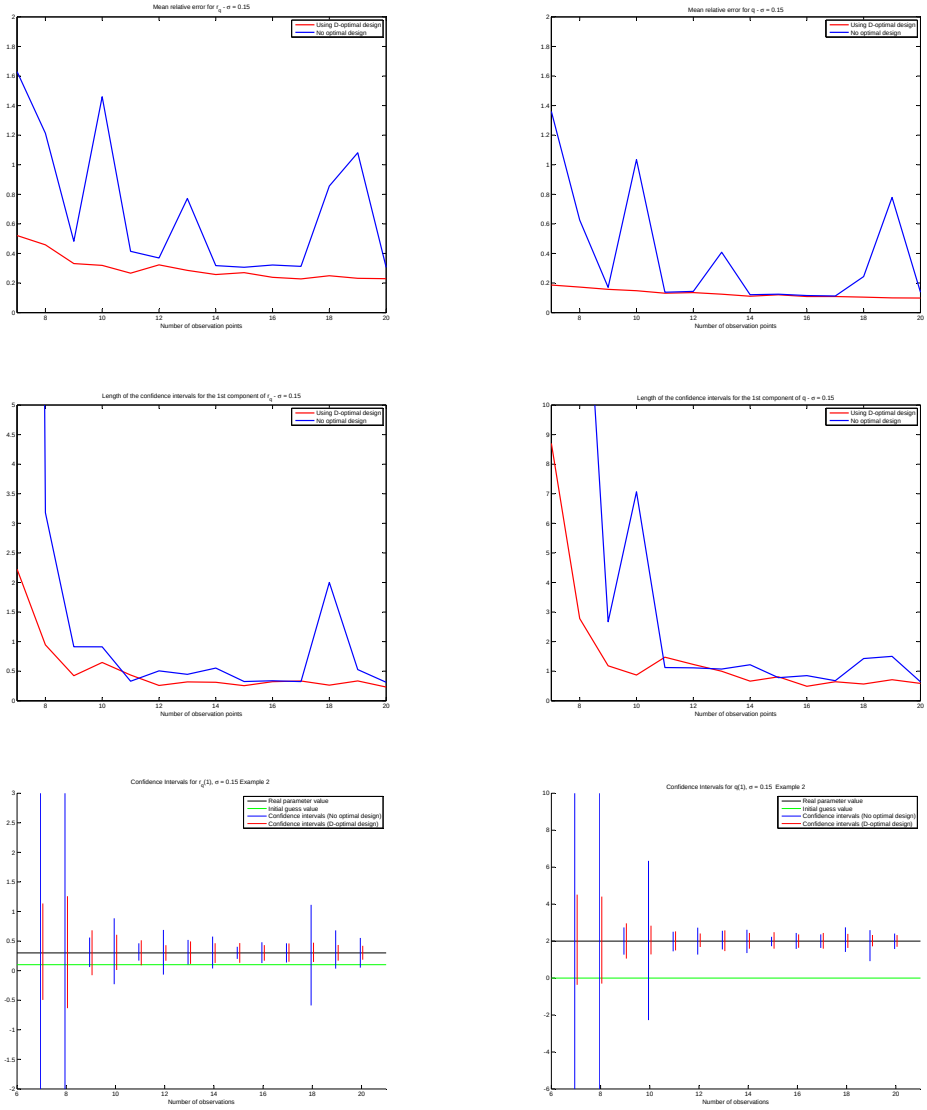

Figure 14: Results for noisy realizations with $\sigma = 0.15$ using D-optimal design (red) and no optimal design (blue). From top to bottom: Mean relative errors $\bar{e}_D(r_q)$ and $\bar{e}_\Lambda(r_q)$ (right) and $\bar{e}_D(q)$ and $\bar{e}_\Lambda(q)$ (left); length of confidence intervals for $r_q(1)$ (right) and $q(1)$ (left); confidence intervals at 90 % confidence level for $r_q(1)$ (right) and $q(1)$ (left).

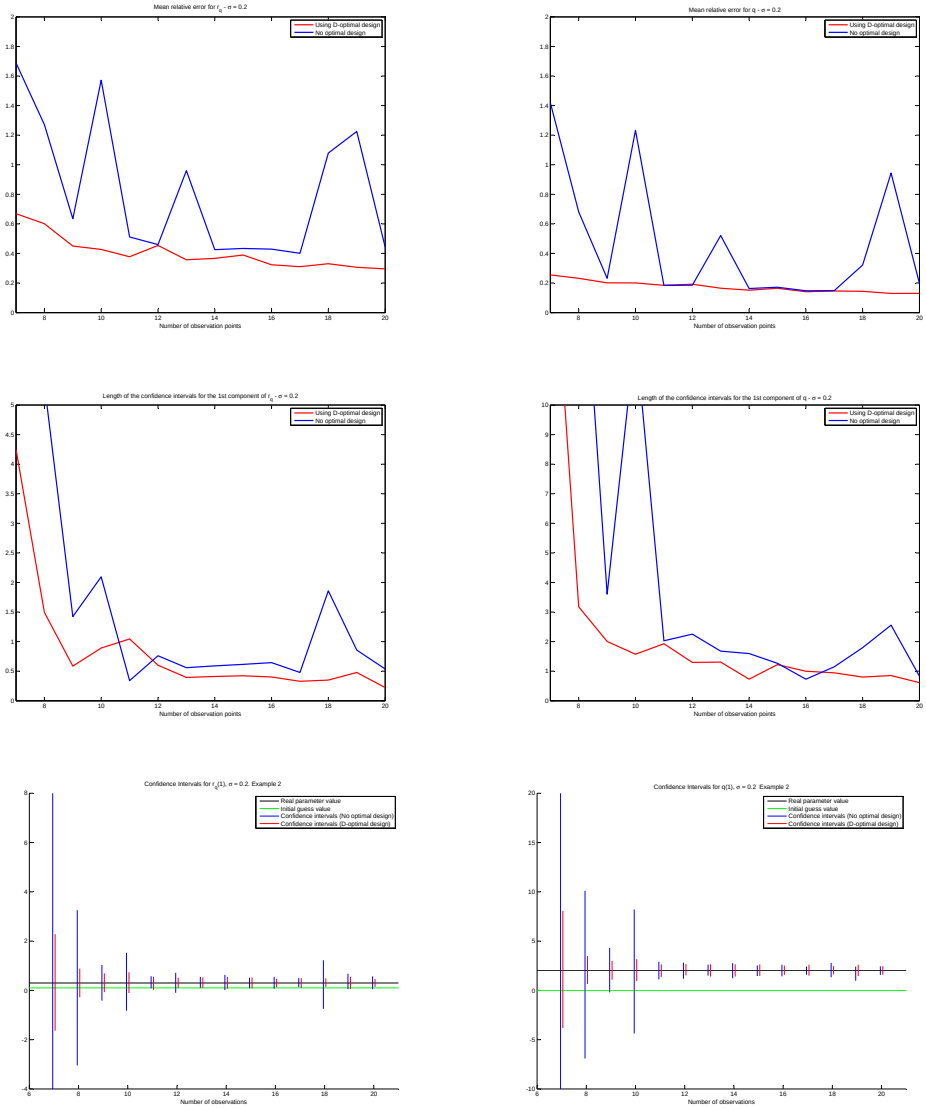

Figure 15: Results for noisy realizations with $\sigma = 0.2$ using D-optimal design (red) and no optimal design (blue). From top to bottom: Mean relative errors $\bar{e}_D(r_q)$ and $\bar{e}_\Lambda(r_q)$ (right) and $\bar{e}_D(q)$ and $\bar{e}_\Lambda(q)$ (left); length of confidence intervals for $r_q(1)$ (right) and $q(1)$ (left); confidence intervals at 90 % confidence level for $r_q(1)$ (right) and $q(1)$ (left).

7 Conclusions

In this paper we have investigated a typical interrogation problem such as those used in EEG. We have shown the value of using some type of optimal design criterion (such as those studied in [6, 7, 8, 11, 12]) in determining how to best collect data. From the numerical results, we would conclude that:

- D-optimal design techniques provide a set observations points leading to a more accurate estimate of the parameters of interest. The results of this paper emphatically demonstrate the benefits of using some type of optimal design criterion (D-optimal in this case) in deciding how data should be collected in a specific application.
- For the specific EEG problem investigated, the length of the confidence intervals as well as the mean relative error do not decrease significantly for more than 10 or 11 observation points. Hence an optimal array of sensors of this size is sufficient in practice. Moreover, there are dramatic differences between estimation accuracies with a smaller number of sensors (≈ 7 or 8) and the optimal values of 10 or 11 sensors.

Acknowledgements

This research was supported in part by the Air Force Office of Scientific Research under grant numbers AFOSR FA9550-12-1-0188 and FA9550-10-1-0037, and in part by the National Institute of Allergy and Infectious Diseases under Grant Number NIAID R01AI071915-10.

References

[1] I. Akduman and R. Kress, Electrostatic imaging via conformal mapping, *Inverse Problems* **18** (2002), 1659–1672.

[2] R.A. Albanese, R.L. Medina and J.W. Penn, Mathematics, medicine and microwaves, *Inverse Problems*, **10** (1994), 995–1007.

[3] R.A. Albanese, J.W. Penn and R.L. Medina, Short-rise-time microwave pulse propagation through dispersive biological media, *J. Optical Society of America A* **6** (1989), 1441–1446.

[4] N. D. Aparicio and M. K. Pidcock, The boundary inverse problem for the Laplace equation in two dimensions, *Inverse Problems*, **12**, (1996), 565–577.

[5] H.T. Banks, M.W. Buksas and T. Lin, *Electromagnetic Material Interrogation Using Conductive Interfaces and Acoustic Wavefronts*, Frontiers in Applied Mathematics, Vol. FR21, SIAM, Philadelphia, PA, 2000.

[6] H.T. Banks, S. Dediu and S.L. Ernstberger, Sensitivity functions and their uses in inverse problems, *J. Inverse and Ill-posed Problems*, **15** (2007), 683–708.

[7] H.T. Banks, S. Dediu, S.L. Ernstberger and F. Kappel, A new optimal approach to optimal design problem, *J. Inverse and Ill-posed Problems*, **18** (2010), 25–83.

[8] H.T. Banks, K. Holm and F. Kappel, Comparison of optimal design methods in inverse problems, CRSC-TR10-11, July 2010; *Inverse Problems*, **27** (2011), 075002.

[9] H. T. Banks, S. Hu, and W. C. Thompson, *Modeling and Inverse Problems in the Presence of Uncertainty*, CRC Press, Boca Raton, FL., 2014.

[10] H. T. Banks and F. Kojima, Boundary shape identification in two-dimensional electrostatic problems using SQUIDs, CRSC-TR98-15, April, 1998; *J. Inverse and Ill-Posed Problems*, **8** (2000), 487–504.

[11] H.T. Banks and K.L. Rehm, Experimental design for vector output systems, CRSC-TR12-11, April, 2012; *Inverse Problems in Sci. and Engr.*, **21** (2013), 1–34. DOI: 10.1080/17415977.2013.797973

[12] H.T. Banks and K.L. Rehm, Experimental design for distributed parameter vector systems, CRSC-TR12-17, August, 2012; *Applied Mathematics Letters,* **26** (2013), 10–14; http://dx.doi.org/10.1016/j.aml.2012.08.003.

[13] H.T.Banks, D. Rubio, N. Saintier and M.I. Troparevsky, Optimal design techniques for distributed parameter systems, CRSC-TR13-01, N. C. State University, Raleigh, NC, January, 2013; *Proceedings 2013 SIAM Conference on Control Theory*, CT13, SIAM, (2013), 83–90.

[14] H.T.Banks, D. Rubio, N. Saintier, M.I. Troparevsky, Optimal electrode positions for the inverse problem of EEG in a simplified model in 3D, MACI, **4** (2013), 521–524. ISSN 2314–3282.

[15] F. Ben Hassen, Y. Boukari and H. Haddar, Inverse impedance boundary problem via the conformal mapping method: the case of small impedances, *Revue ARIMA*, **13** (2010), 47–62.

[16] M. Clerc, J. Leblond, J-P Marmorat and T. Papadopoulo, Source localization using rational approximation on plane sections, *Inverse Problems*, **28** (2012), 1–24.

[17] D. Colton and R. Kress, *Inverse Acoustic and Electromagnetic Scattering Theory*, Springer Applied Mathematical Sciences, Vol. 93, 3rd ed., Springer Verlag, 2013.

[18] D. Colton, R. Kress and P. Monk, A new algorithm in electromagnetic inverse scattering theory with an application to medical imaging, *Math Methods Applied Science*, **20** (1997), 385–401.

[19] J.C. de Munck, The potential distribution in a layered anisotropic spheroidal volume conductor, *J. Appl. Phys.*, **64** (1988), 464–470.

[20] J.C. de Munck, H. Huizenga, L.J. Waldrop, and R.M. Heethaar, Estimating stationary dipoles from MEG/EEG data contaminated with spatially and temporal correlated background noise, *IEEE Trans. On Signal Processing*, **50** (2002), 1565–1572.

[21] A. El Badia, A inverse source problem in an anisotropic mdium by boundary measurements, *Inverse Problems*, **16** (2000), 651–663.

[22] A. El Badia, Summary of some results on an EEG inverse problem, *Neurology and Clinical Neurophysiology*, **2004** (2004), 102.

[23] A. El Badia and M. Farah, Identification of dipole sources in an elliptic equation from boundary measurements: application to the inverse EEG problem, *J. Inv. Ill-Posed Problems*, **14**, (2006), 331–353.

[24] C. Gabriel, S. Gabriel and E. Corthout, The dielectric properties of biological tissues: I. Literature survey, *Phys. Med. Biol.* **41** (1996), 2231–2249.

[25] S. Gabriel, R.W. Lau and C. Gabriel, The dielectric properties of biological tissues: II. Measurements in the frequency range 10 Hz to 20 GHz, *Phys. Med. Biol.* **41** (1996), 2251–2269.

[26] S. Gabriel, R.W. Lau and C. Gabriel, The dielectric properties of biological tissues: III. Parametric models for the dielectric spectrum of tissues, *Phys. Med. Biol.* **41** (1996), 2271–2293.

[27] M. Hamalainen, R. Hari, R.J. Ilmoniemi, J. Knuutila and O. Lounasmaa, Magnetoencephalography, theory, instrumentation and applications to noninvasive studies of the working human brain, *Reviews of Modern Physics*, **65** (1993), 414–487.

[28] H. Huizenga, J.C. de Munck, L.J. Waldrop, and R.P. Grasman, Spatiotemporal EEG/MEG source analysis based on a parametric noise covariance model, *IEEE Trans. Biomedical Engineering*, **49** (2002), 533–539.

[29] R. Kress, Inverse Dirichlet problem and conformal mapping, *Mathematics and Computers in Simulation*, 2004 DOI:10.1016/j.matcom.2004.02.006

[30] R. Kress and W. Rundell, Nonlinear integral equations and the iterative solution for an inverse boundary value problem, *Inverse Problems*, **21** (2005), 1207-1223.

[31] J.C. Mosher, R.M. Leahy and P.S. Lewis, EEG and MEG: Forward solutions for inverse methods, *Trans. Biomedical Engineering*, **46** (1999), 245–259.

[32] D. Rubio and M. I. Troparevsky, The EEG forward problem: theoretical and numerical aspects, *Latin American Applied Research*, **36** (2006), 87–92.

[33] J. Sarvas, Basic mathematical and electromagnetic concepts of the biomagnetic inverse problem, *Phy. Med Biol.*, **32** (1987), 11–22.

[34] P. H. Schimpf, C. Ramon and J. Haneisen, Dipole models for EEG and MEG, *IEEE Trans. Biomedical Engineering*, **49** (2002), 409–418.

[35] G.A.F. Seber and C.J. Wild, *Nonlinear regression*, Wiley Intersciences, Hoboken , NJ, 2003.

[36] M.I. Troparevsky and D. Rubio, On the weak solutions of the forward problem in EEG, *J. of Applied Mathematics*, **12** (2003), 647–656.

[37] M.I. Troparevsky and D. Rubio, Weak solutions of the forward problem in EEG for different conductivity values, *Mathematical and Computer Modeling*, **41** (2005), 1403–1492.

[38] I.S. Yetik, A. Nehorai, C.H. Muravchik, J. Haueisen, Line-source modeling and estimation with magnetoencephalography, *IEEE Trans. Biomed. Eng.*, **52**, (2005), 839–851.